Nanoscale

Accepted Manuscript

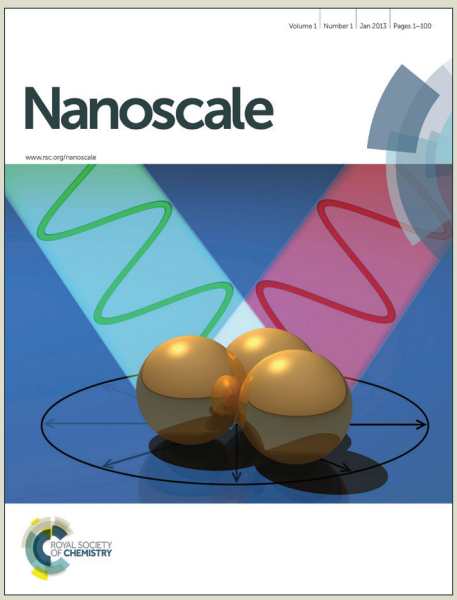

ROYAL SOCIETY OF CHEMISTRY

www.rsc.org/nanoscale

Photodynamic effect of functionalized single-walled carbon nanotubes: a potential sensitizer for photodynamic therapy

Lei Wang, Jinjin Shi, Ruiyuan Liu, Yan Liu, Jing Zhang, Xiaoyuan Yu, Jun Gao, Chaofeng Zhang, Zhenzhong Zhang*

School of Pharmaceutical Sciences, Zhengzhou University, 100 Kexue Avenue, Zhengzhou, 450001, PR China.

* Correspondent: Prof. Zhenzhong Zhang. Tel: 86-371-67781910; Fax: 86-371-67781908; Email: zhangzz08@126.com

Abstract

Single-walled carbon nanotubes (SWNTs) possess unique physical and chemical properties, which make them very attractive for a wide range of applications. In particular, SWNTs and their composites have shown a great potential for photodynamic therapy (PDT). People usually used SWNTs for photothermal therapy, herein, the photodynamic effect of two functionalized SWNTs were detected under visible light illumination in vitro and in vivo. The results indicated that the photodynamic effect is not entirely dependent on illumination time, but also on the modification methods of SWNTs. The ability of SWNTs complexes to combine the photodynamic therapy significantly improved the therapeutic efficacy of cancer treatment, and the combined treatment demonstrated a synergistic effect. These findings suggest that SWNTs composite has a great potential as sensitizer for PDT.

1 Introduction

As of 21st century, cancer is arguably the most complex and challenging disease known to mankind and an inevitable public health concern of this millennium. The ultimate goal of cancer therapeutics is to increase the survival time and the quality of life of the patient by reducing the unintended harmful side-effects. [1] The most common types of cancer treatment are chemotherapy, radiation and surgery. [2] In recent years, photodynamic therapy (PDT) has attracted considerable attentions. PDT is a minimally invasive and promising new method in cancer treatment, [3-6] which uses special photosensitizer (PS) along with visible light to kill cancer cells. This approach utilizes reactive oxygen species (ROS) generated by the tissue-localized non-toxic PS upon illumination and in the presence of oxygen. [7-9] As well known, cancer cells have the increased ROS levels compared to normal cells, and the increased ROS levels allow for activation of several signaling pathways that could be beneficial to cancer cells. However, excessive ROS can lead to DNA damage causing apoptosis. For most PS employed in PDT, ROS play a major role in killing cancer cells. [10, 11]

With the development of cancer nanotechnology, researchers have focused on developing nano-scale anticancer drug carriers for improving therapeutic efficacy as well as reducing unwanted side effects [12]. Single-walled carbon nanotubes (SWNTs) possess splendid potential applications in modern science and technology due to their unique chemical and physical characteristics endowed by their novel nanostructures. [13-15] In particular, those ones that employ SWNTs for DNA, siRNA, proteins technologies and drug delivery for biomedical applications have attracted much

attentions. [16-19] Although non-functionalized SWNTs have apparent toxicity to cells and animals [20, 21], properly functionalized SWNTs are able to enter cells and shuttle various biological molecular cargoes into cells without toxicity. [22]

Recent researches on SWNT-based therapeutics have emphasized the photothermal effect under NIR irradiation. [19, 23-25] To date, only a few of studies report on the photodynamic effect of SWNTs. In view of the modified Jablonski diagram for SWNTs, the photodynamic effect should be considered because SWNTs are a mixture of metallic and semiconducting SWNTs [26].

Herein, two types of functionalized SWNTs used as PS are reported. SWNTs covalently functionalized with PEI (SWNT-PEI) and non-covalently functionalized with PVPk30 (SWNT- PVPk30) were prepared and characterized. The aim of the present study was to detect the potential photodynamic effect and mechanism of SWNT-PEI and SWNT-PVPk30 on mice melanoma B16-F10 cells.

2 Experimental section

SWNTs used in the present study were purchased from Chengdu Organic Chemicals Co. Ltd. (produced by chemical vapor deposition process (CVD), purity >90%, Lot No. 1109). Mice melanoma B16-F10 cell line was obtained from American Type Culture Collection (ATCC, No. CRL-6475) and all other reagents were bought from Sigma-Aldrich Co. LLC.

2.1 Preparation of SWNT-PEI

Pristine SWNTs (100 mg) were suspended in 12 M HNO_3, and stirred for 24 h at

room temperature. The purified SWNTs were then collected on a membrane filter (Millipore, pore size 100 nm). Then heated the purified SWNTs to 110 ℃ under reflux in 100 ml of 4 M HNO_3 for 2 h, followed by filtration on a membrane filter and multiple washes with Milli-Q water. The remaining solid was suspended in 1 M HCl in an ultrasonic bath for about 30 min, diluted by Milli-Q water and the washing steps were repeated. Consequently the purified SWNTs were decorated with carboxylic acid groups (SWNT-COOH), and then heated to dryness at 110 ℃.

SWNT-COOH (50 mg) was suspended in 20 ml thionyl chloride ($SOCl_2$, containing 1 ml of anhydrous dimethylformamide (DMF)). Then the mixture was heated under reflux for 24 h to convert the carboxylic acids to acyl chlorides. These nanotubes were rinsed over a PTFE membrane (Millipore, pore size 100 nm) with anhydrous THF to remove excess $SOCl_2$, and were then added to ethylenediamine (EDA) and stirred for 3-5 days in order to form SWNT-NH_2. The remaining solid was dried under vacuum at room temperature.

For preparation of SWNT-PEI, SWNT-NH_2 was immersed in $SOCl_2$, and then aziridine and a certain amount of HCl were added. The mixture was left in an ultrasonic bath for about 30 min. The solution was heated to reflux for 24 h under nitrogen. The resultant was thoroughly washed with copious $SOCl_2$ and sonicated in methanol. Finally the washed substrate was dried in vacuum at room temperature.

2.2 Preparation of SWNT-PVPk30

For non-covalent functionalization, 50 mg SWNTs were purified and suspended in the aqueous solution of 10 mg/ml PVPk30 and sonicated using an ultrasonic probe

(400 w × 10 times). The suspension was then filtered through a membrane filter (Whatman, pore size 100 nm) to remove excess surfactants, rinsed thoroughly with ultra-pure H_2O. The amount of PVPk30 on the surface of SWNTs was detected at 247 nm (UV-3600, Shimadzu, Japan) [22].

2.3 Characterization

Functionalized SWNTs was investigated by fourier transform infrared spectrum (FT-IR, Nicolet iS10, Thermo), nuclear magnetic resonance spectrum (NMR, DMX-500, Bruker) and thermogravimetric analysis (TGA, Pyris1, PerkinElmer). The size and morphology of the two types of functionalized SWNTs were characterized by using a transmission electron microscopy (TEM, Tecnai G2 20, FEI) and an atomic force microscopy (AFM, Shimadzu，9500J3，Japan).

2.4 Illumination treatment

Illumination treatment was conducted under a commercial 500 W tungsten halogen lamp (wavelength range: 300~2600 nm) with a piece of insulated glass with a distance of 20 cm.

2.5 DNA cleavage experiments

The DNA cleaving ability was assayed by using EGFR plasmid DNA as a substrate in Tris-HCl (50 mM, pH 7.4) in the presence of SWNT-PEI and SWNT-PVPk30 (SWNTs ≈ 50 μg/ml) with or without illumination. Absorbance at 808 nm (A808) was used to determine the SWNTs concentration in the suspension by visible spectrophotometry (UV-3600, Shimadzu, Japan) [27].

To verify the mechanism of DNA cleavage promoted by functionalized SWNTs

with illumination, typical ROS scavengers including hydroxyl radical scavengers (*t*-BuOH), singlet oxygen scavenger (NaN_3) and superoxide scavenger (KI) were added to the system. The cleaved DNA products were immediately run on a 0.8% agarose gel and images were obtained from a GelDoc 2000 imager system (Bio-Rad, Munich, Germany).

2.6 Cellular uptake, nuclear translocation and cytotoxicity

0.1 ml fluorescein isothiocyanate (FITC) in dimethyl sulfoxide (1 mg/ml) was added to 5 ml SWNT-PEI or SWNT-PVPk30, and these mixtures were then sonicated with protection from light. Gel chromatography was used to remove the excess FITC by a Sephadex G-25 column (Sigma). B16-F10 cells were cultured in normal RPMI-1640 culture medium with 10% fetal bovine serum (FBS) and 1% penicillin/streptomycin at 37 ℃, 5% CO_2 in an incubator (MCO-15AC, Sanyo). The cells were plated into chambered cover-slides 24 h prior to incubation at a density of 1 $\times 10^5$ cells/well. FITC alone, SWNT-PEI/FITC and SWNT-PVPk30/FITC were added to the above plate wells. The concentration of SWNTs was about 50 μg/ml. The cells were incubated at 37℃ for 2, 4 and 6 h. After incubation, the cells were washed twice with PBS and tracked their internalization into the cells through colocalization of FITC-signal (green fluorescence), and then detected the changes of FITC-signal using a Flow Cytometry (FCM, Epics XL.MCL).

A CLSM (Leica, TCSSP5, Germany) was used to evaluate the cellular uptake and intracellular distribution of complexes incubated with B16-F10 cells. B16-F10 cells (1×10^5) were seeded on chambered cover-slides with RPMI-1640 medium for

24 h. The cells were treated with various complexes formulations. The concentrations of SWNTs was about 50 μg/ml, respectively. After the cells were incubated, cells were rinsed with cold PBS three times and fixed with 4% paraformaldehyde for 15 min at 37 ℃. Next, Hoechst 333258 (5 mg/ml) was added for 20 min at 37 ℃. After the staining solution was removed, the cells were rinsed with PBS three times. After staining of the nucleus, the cells were observed by CLSM.

B16-F10 cells were plated in 96-well plates and incubated for 24 h, then treated with SWNT-PEI or SWNT-PVPk30 at different concentrations (10, 20, 30, 40, 50, 60, 70, 80 μg/ml). After 6 h incubation, the cells were or were not subject to illumination for 2 h. After another 24 h culture, cytotoxicity was measured by sulforhodamine B assay (SRB).

2.7 Comet Assay

To determine the DNA damaging effect, B16-F10 cells were seeded into 6-well plates and incubated overnight. Cells were treated with SWNT-PEI and SWNT-PVPk30 (SWNTs ≈ 50 μg/ml). After 6 h treatment, the cells were then subject to illumination for 2 h. After 24 h incubation, the cells were washed with PBS, scrapped, centrifuged, and resuspended in 100 μl PBS. The comet assay was performed by Comet Assay Kit (Trevigen, Gaitherburg, MD, USA) according to the manufacturer's instructions. The slides were coded, and one scorer performed the comet analysis using a fluorescence microscopy (Zeiss LSM 510). At least 90 cells per sample (three replicates, each with 30 cells per slide) were analyzed using the comet image analysis software, and the percentage of DNA, tail length and tail moment in the comet tail were used as a

measure of the amount of DNA damage. We used B16-F10 cells exposed to H_2O_2 as a positive control and untreated cells as a negative control.

2.8 ROS assay

Intracellular ROS levels were measured using a fluorescent dye dichlorodihydrofluorescin diacetate (DCFH-DA), which could be rapidly oxidized into the highly fluorescent 2′,7′-dichlorofluorescein (DCF) in the presence of intracellular ROS. B16-F10 cells were plated in 6-well plates and incubated for 24 h, then treated with SWNT-PEI or SWNT-PVPk30. After 4 h treatment, the cells were then subject to illumination. Then washed cells with RPMI-1640 medium (without FBS), and incubated the cells with DCHF-DA (10 μM) 1 ml at 37 ℃ for 30 min. The resultants were observed by fluorescence microscopy (Zeiss LSM 510) and the fluorescence intensity was measured under an excitation at 488 nm and emission at 525 nm using a fluorescence microplate reader (BioTek, USA). ROS levels were expressed as fold change over control.

2.9 Determination of glutathione (GSH) levels

The levels of GSH in the B16-F10 cells were quantified using monochlorobimane (mBCL). After treatment with SWNT-PEI and SWNT-PVPk30 for 4 h, the cells were then subject to illumination. B16-F10 cells were harvested from culture dishes and suspended in PBS. A 50 mM stock solution of mBCl was prepared in dehydrated alcohol and kept in the dark at −20 ℃ until needed. It was added to serum-free RPMI-1640 medium to give a final concentration of 40 μM. It was incubated for 20 min at 37℃ and fluorescence of the GSH-mBCl adduct was measured at an

excitation at 390 nm and emission at 478 nm using a fluorescence microplate reader (BioTek, USA). The fluorescence images were examined by fluorescence microscopy (Zeiss LSM 510).

2.10 Western blot analysis

Western blot analysis was performed to determine the expression levels of p53, Bax, Bcl-2 and p-Bad proteins in untreated, SWNT-PEI-treated, and SWNT-PVPk30-treated cells. Cells were harvested after treatment, washed with cold PBS (pH 7.4) and lysed with RIPA lysis buffer. In separate experiments, the membrane was incubated with mouse monoclonal anti-p53 antibody (1:1000 dilution, Santa Cruz, sc-126), mouse monoclonal anti-Bax antibody (1:1000 dilution, Santa Cruz, sc-70407), mouse monoclonal anti-Bcl-2 antibody (1:1000 dilution, Santa Cruz, sc-7382) and mouse monoclonal anti-β-actin antibody (1:1000 dilution, Santa Cruz, sc-47778) overnight at 4 ℃. After washing with Tris–buffered saline containing 0.1% Tween-20, the membranes were then incubated with HRP conjugated anti-mouse secondary antibody (1:2000 dilution). Blots were visualized with the BeyoECL plus detection system.

2.11 Apoptosis assay

Changes in cell morphology were analyzed using fluorescence microscopy. To determine cellular apoptosis, 1×10^5 B16-F10 cells were seeded into 6-well plastic plates and incubated overnight. Cells were treated with SWNT-PVPk30 or SWNT-PEI suspension for 4 h. The illumination treatment was same as the step of "Illumination treatment". After culture for 24 h, the cells were resuspended in 500 μl binding buffer,

then stained with 5 μl Annexin V-FITC and 5 μl propidium iodide (PI) for 15 min in darkness, finally analyzed by a flow cytometer (FCM, Epics XL, MCL).

2.12. Photodynamic therapy efficiency of SWNT-PEI *in vivo*

All animal experiments were performed under a protocol approved by Henan laboratory animal center. Mice melanoma tumor models were generated by subcutaneous injection of 1×10^6 B16-F10 cells in 0.1 ml saline into the right shoulder of female C57 mice (18~22 g, Henan laboratory animal center). The mice were used when the tumor volume reached 60~100 mm^3 (about 5 days after tumor inoculation).

The mice were divided into 6 groups (5 mice per group): control group, control in dark group, SWNT-PEI+illumination group, SWNT-PEI in dark group SWNT-PVPk30+illumination group and SWNT-PVPk30 in dark group. 0.2 ml of SWNT-PEI (SWNT dose: 50 μg/ml) in saline were by in situ injection injected into mice every 2 days. Injection of all complexes at multiple sites inhibited the growth of tumor. For the illumination treatment, we used 300 W tungsten-halogen lamp for the entire treatment process. The mice were observed daily for clinical symptoms and the tumor sizes were measured. After treatment for 10 days, the mice were killed to collect tumor, and the collected tissues were soaked in 10% formalin solution, embedded with paraffin, embedded with paraffin for H&E staining. Morphological changes were observed under microscopy (Zeiss LSM 510). (Zeiss LSM 510).

2.13 Statistical analysis

Quantitative data were expressed as Mean ± SD and analyzed by an analysis of variance (ANOVA) followed by Dunnett post test. *P* values of <0.05 were considered

statistically significant.

3 Results and discussion

3.1 Functionalization and Characterization of SWNT-PEI and SWNT-PVPk30

Raw carbon nanotubes have highly hydrophobic surfaces, and are not soluble in aqueous solutions. For biomedical applications, surface functionalization is required to solubilize SWNTs, render biocompatibility and low toxicity [28-30]. In this study, two types of functionalized SWNTs were used.

For covalent functionalization, SWNTs were functionalized with polymerised PEI (SWNT-PEI), which was performed by a cationic polymerization of aziridine in the presence of amine-functionalized SWNTs (SWNT-NH_2). The analysis of FT-IR, NMR and TGA (Fig. 1) showed that the functionalized SWNT-PEI was obtained. FT-IR spectrum showed no significant changes in the basic structure of pristine SWNTs (Fig. 1a) after carboxylation (Fig. 1b) and amination (Fig. 1c). However, typical peaks at 1715 cm^{-1} for carboxyl group and at 1630 cm^{-1} for primary amine were found after carboxylation and amination of SWNTs, respectively. The typical peaks at 600~800 cm^{-1} and 3729 cm^{-1} indicated the attachment of amidogen to SWNTs. Comparison of ^1H NMR spectrum (Fig. 1d) of SWNT-PEI in D_2O with that of PEI in D_2O (pH 7.0) indicated that polymerized PEI on the surface of SWNTs and pure PEI have the same chemical shift at 3.6～3.7 (ppm). Due to the protonation, the typical peak of SWNT-PEI is significantly downsized. The amount of PEI attached to SWNTs was investigated by TGA. SWNTs were stable up to 675 ℃, while pure PEI

was absolutely degraded at about 525 ℃. At 525 ℃, the weight loss of SWNTs, SWNT-NH_2 and SWNT-PEI were 0, ~1.2% and ~9.35%, respectively, thus the weight ratio of PEI on the surface of SWNTs was ~8.15% (Fig. 1e).

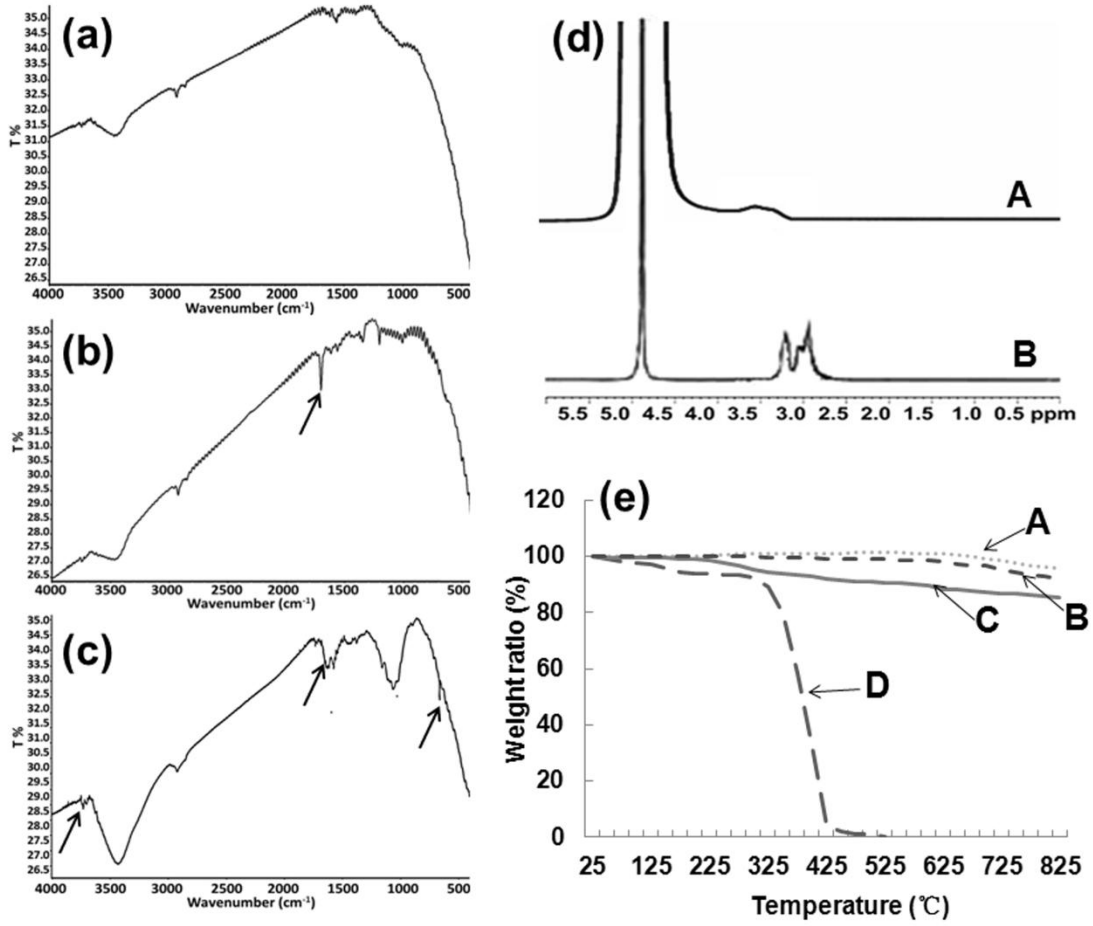

Fig. 1 FT-IR spectrum of **a)** pristine SWNTs, **b)** SWNT-COOH and **c)** SWNT-NH_2. **d)** ^{1}H NMR spectrum of (A) SWNT-g-PEI and (B) PEI. **e)** TGA curves of (A) pristine SWNTs, (B) SWNT-NH_2, (C) SWNT-g-PEI and (D) PEI.

For non-covalent functionalization, PVPk30 was used as a surfactant with equal amounts to SWNTs. The AFM and TEM results indicated that SWNT-PEI and SWNT-PVPk30 were uniform. The aqueous solutions of the two functionalized SWNTs were both stable even months (Fig. 2).

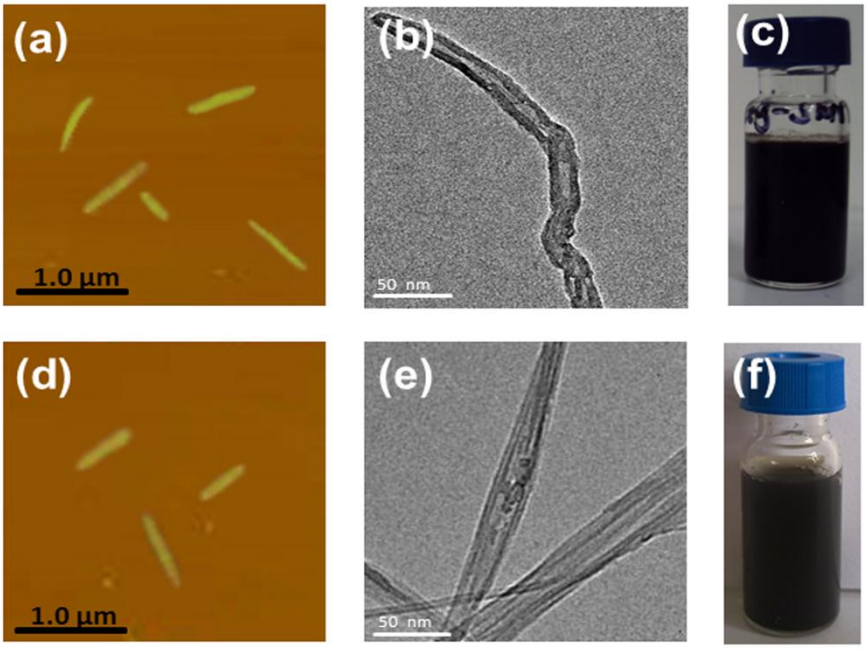

Fig. 2 AFM pictures of (a) SWNT-PEI and (d) SWNT-PVPk30; TEM pictures of (b) SWNT-PEI and (e) SWNT-PVPk30; photos of (c) SWNT-PEI and (f) SWNT-PVPk30 in water.

3.2 DNA cleavage by SWNT-PEI and SWNT-PVPk30

The DNA cleavage activity of SWNT-PEI and SWNT-PVPk30 was determined by agarose gel electrophoresis. The band of DNA control was observed in Fig. 3a-1 (Form Ⅰ). As shown in Fig. 3, no band of form Ⅱ in DNA+2h illumination(Fig. 3a-2), DNA+PEI+2h illumination (Fig. 3a-3), DNA+PVPk30+2h illumination (Fig. 3a-4), DNA+SWNT-PEI (Fig. 3b-1, 3, 5) and DNA+SWNT-PVPk30 (Fig. 3c-1, 3, 5) groups was observed, demonstrating SWNT-PEI (without illumination), SWNT-PVPk30 (without illumination), PEI and PVPk30 do not induced DNA cleavage obviously. The results were consistent with Andrea`s resport that PEI nanocarriers do not induce mutations nor oxidative DNA damage. [31] However, after treatment with SWNT-PEI (Fig. 3b-6) or SWNT-PVPk30 (Fig. 3c-6) for 0.5 h illumination, the Form Ⅰ band became weaker, and the Form Ⅱ band was observed. With prolongation of the

illumination time, the Form Ⅰ bands were gradually disappeared. When the illumination time reached 2 h (Fig. 3b-2), the Form Ⅰ band in the SWNT-PEI with illumination group was disappeared completely (2 h used as working illumination time in this study).

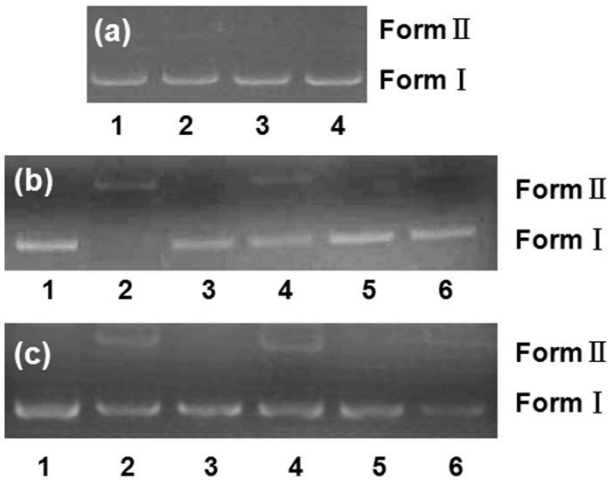

Fig. 3 Gel electrophoresis diagram showing the photoinduced cleavage.

(a) a-1: blank plasmid DNA; a-2: plasmid DNA+2h illumination; a-3: plasmid DNA+PEI+2h illumination; a-4: plasmid DNA+PVPk30+2h illumination; **(b)** b-1, 3, 5 were DNA+SWNT-PEI without illumination; b-2, 4, 6 were DNA+SWNT-PEI with illumination for 2, 1 and 0.5 h; **(c)** c-1, 3, 5 were DNA+SWNT-PVPk30 without illumination; c-2, 4, 6 were DNA+SWNT-PVPk30 with illumination at 2, 1 and 0.5 h.

The similar results were appeared in SWNT-PVPk30 with illumination group, but with prolongation of the illumination time, the DNA cleavage ability was not significantly strengthened, indicating that the DNA cleavage ability of SWNT-PEI was stronger than SWNT-PVPk30, and the weakened effect of SWNT-PVPk30 on DNA cleavage may be due to the covering of PVPk30.

To verify the mechanism of DNA cleavage promoted by visible light

illumination, typical ROS scavengers were added to the system. As shown in Fig. 4, evident inhibition effect on the DNA cleavage was observed in the presence of every scavenger, showing that the DNA cleavage may occur through a ROS pathway.

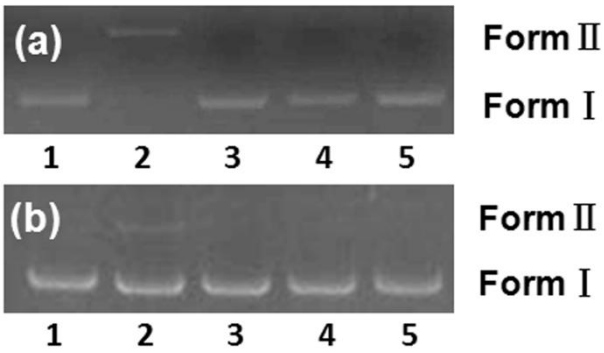

Fig. 4 Agarose gel electrophoresis assays for the effect of ROS scavengers on the cleavage reaction. **(a)** a-1: DNA control; a-2: DNA+SWNT-PEI+2 h illumination; a-3~5: DNA+SWNT-PEI+2 h illumination+NaN_3, t-BuOH or KI; **(b)** b-1: DNA control; b-2: DNA+SWNT-PVPk30+2 h illumination; b-3~5: DNA+SWNT-PVPk30+2h illumination+NaN_3, t-BuOH or KI.

3.3 Cellular uptake and of SWNT-PEI and SWNT-PVPk30

Flow cytometry analysis was carried out to evaluate endocytosis of FITC-labeled SWNT-PEI and SWNT-PVPk30. No change for FITC signal in the cells treated with FITC alone was found with increasement of incubation time. However, while the cells were treated with SWNT-PEI (Fig. 5a) or SWNT-PVPk30 (Fig. 5b), the signals in the cells were increased with prolongation of the incubation time, indicating that the uptake of SWNT-PEI or SWNT-PVPk30 by B16-F10 cells was time-dependent. While SWNT-PEI completely entered into the cells at 4 h, the fluorescence intensity of SWNT-PVPk30 was the highest at 6 h, suggesting that SWNT-PEI and SWNT-PVPk30 can enter into B16-F10 cells effectively.

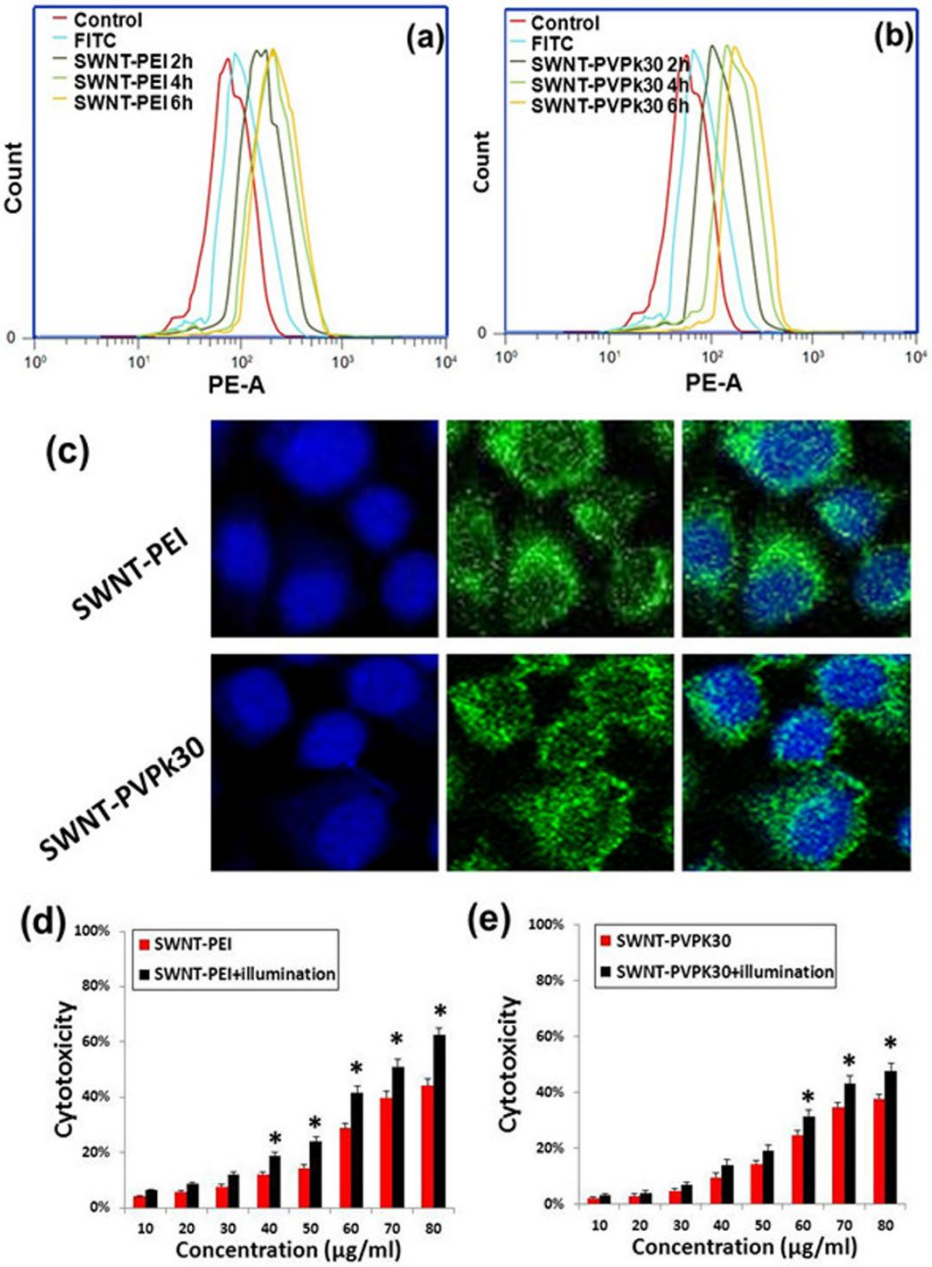

Fig. 5 **(a)** B16-F10 cells uptake of FITC and SWNT-PEI/FITC at 2, 4 and 6 h; **(b)** B16-F10 cells uptake of FITC and SWNT-PVPk30/FITC at 2, 4 and 6 h. **(c)** CLAM images for uptake in B16-F10 cells incubated with SWNT-PEI and SWNT-PVPk30. The concentration of SWNTs was 50 μg/ml. Cell nuclei were counterstained with Hoechst 333258 (blue). **(d)** and **(e)** were the cytotoxicity of SWNT-PEI and SWNT-PVPk30 with or without lamp illumination treatment for 2 h. (Mean ± SD, n = 3, $p < 0.05$) (*) indicates statistically significant between with illumination and without illumiantion groups.

The nuclear translocation of SWNT-PEI and SWNT-PVPk30 was studied by CLSM after FITC-labeled complexes incubated with B16-F10 cells (Fig. 5c). The green fluorescence was found in the nucleus, illustrating that the two complexes can make the efficacy of the nuclear translocation in the B16-F10 cells.

The SRB results showed that SWNT-PEI (Fig. 5d) and SWNT-PVPk30 (Fig. 5e) had no significant cytotoxicity to the B16-F10 cells at a concentration of less than 50 μg/ml (used as working concentration), however, a significant difference appeared under the above conditions with exception of illumination ($P < 0.05$).. The cytotoxicity of cells treated with SWNT-PEI+illumination or SWNT-PVPk30+illumination was both increased significantly compared with no illumination groups.

3.4 Detection of DNA damage by comet assay

To evaluate the effect of SWNT-PEI or SWNT-PVPk30 exposure on DNA damage, we then detected DNA fragmentation by comet assay. Percentage of DNA tail is an important parameter in evaluating DNA damage in the cells.

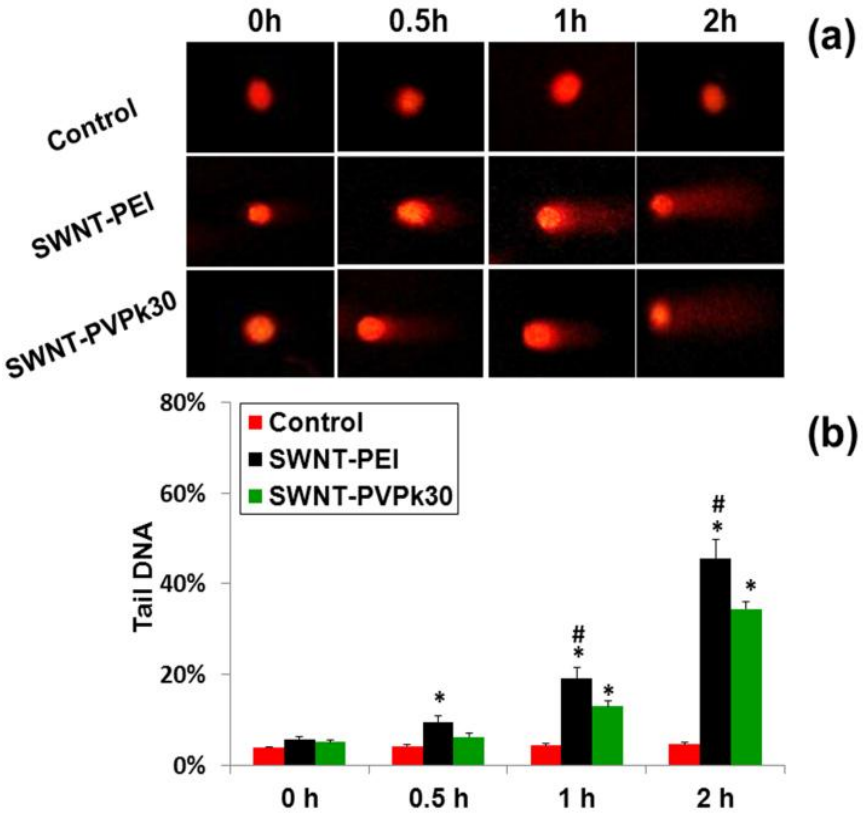

Fig. 6 **(a)** Comet assay of B16-F10 cells exposed to SWNT-PEI or SWNT-PVPk30 suspension with 0 h, 0.5, 1 and 2 h lamp illumination. **(b)** Tail DNA analysis of B16-F10 cells exposed to SWNT-PEI or SWNT-PVPk30. (Mean ± SD, n = 3, $p < 0.05$). (*) indicates statistically significant from control; ($^{\#}$) indicates statistically significant between SWNT-PEI and SWNT-PVPk30 groups.

As shown in Fig. 6, no significant DNA damage was observed in control group. For SWNT-PEI and SWNT-PVPk30 without illumination, no obvious DNA damage was found at the concentration of 50 μg/ml.

With the increase of illumination time, DNA damage in SWNT-PEI and SWNT-PVPk30 groups were enhanced, however, more DNA damage in SWNT-PEI group was found compared with SWNT-PVPk30 group, suggesting that DNA damage is not entirely dependent on illumination time, but also on the modification methods of SWNTs.

3.5 Determination of ROS production and GSH reduction

As ROS are known to cause DNA damage and cell inhibition [32, 33], whereby insufficient cellular repair mechanisms induce additional changes in DNA of tumor cells to make those cells apoptosis or death. And GSH is the most abundant thiol-containing peptide in the cell and a known scavenger of a broad range of ROS [34].

To explore the mechanism of DNA damage by SWNT-PEI or SWNT-PVPk30, the effects of SWNT-PEI or SWNT-PVPk30 (SWNTs ≈ 50 μg/ml) on ROS generation and GSH level were determined. As shown in Fig. 7, the fluorescence of blank cells were not changed under illumination, and no significant fluorescence intensity was observed in SWNT-PEI and SWNT-PVPk30 groups without illumination compared with control group, indicating that no ROS generation was found. However, there were significantly differences between SWNT-PEI (or SWNT-PVPk30) group with illumination and SWNT-PEI (or SWNT-PVPk30) with illumination for 1 and 2 h ($P < 0.05$). Both SWNT-PEI and SWNT-PVPk30 with illumination treatment significantly increased the ROS generation with a illumination time-related manner. In addition, GSH levels of SWNT-PEI and SWNT-PVPk30 with illumination group were decreased with prolonged illumination time (Fig. 8). The ROS level of cells treated with SWNT-PVPk30 was obviously weaker and GSH was stronger than that of SWNT-PEI group at 1 and 2 h ($P < 0.05$).

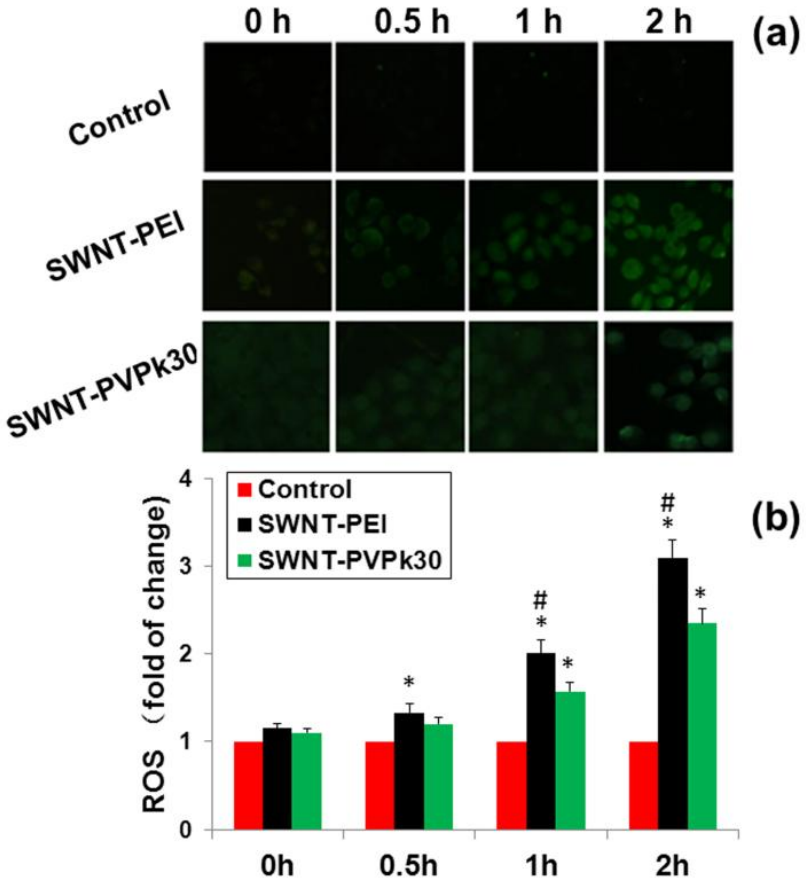

Fig. 7 Treatment with SWNT-PEI or SWNT-PVPk30 under illumination resulted in significant increases in ROS generation in B16-F10 cells. **(a)** Analysis of ROS was performed using a fluorescence microscopy. **(b)** The data are expressed as fold change over control. (Mean ± SD, n = 3, $P < 0.05$). (*) indicates statistically significant from control; ($^{\#}$) indicates statistically significant between SWNT-PEI and SWNT-PVPk30 groups.

For most photosensitizers employed in photodynamic therapy, ROS play a major role in killing cancer cells. Murakami etc. reported that under near-infrared laser irradiation, SWNTs generated ROS [35]. In this study, we used tungsten halogen lamp (wavelength range: 300~2600 nm) for illumination, and the results indicated that illumination treatment alone of B16-F10 cells has no effect on ROS and GSH generation. However, the effect of SWNT-PEI with illumination on ROS generation

and GSH level were stronger and weaker than that of SWNT-PVPk30, respectively. It may be due to the different functionalization on the surface of SWNTs, indicating that SWNT-PEI may be a promising PDT carrier.

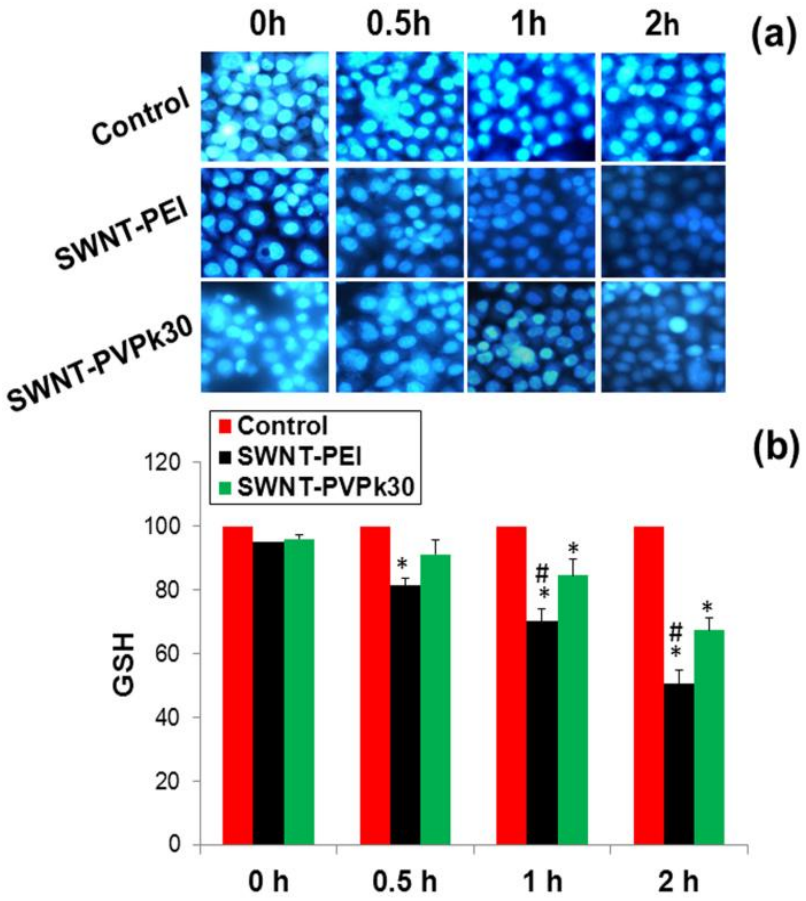

Fig. 8 **(a)** Fluorescence images show reduced GSH levels for exposure of cells to SWNT-PEI or SWNT-PVPk30 with illumination treatment; **(b)** decreased GSH levels in a concentration and illumination time-related manner (Mean ± SD, n = 3, $p < 0.05$). (*) indicates statistically significant from control; ($^{\#}$) indicates statistically significant between SWNT-PEI and SWNT-PVPk30 groups.

3.6 Modulation of pro-and anti-apoptotic proteins

Treatment of cells with SWNT-PVPk30 and SWNT-PEI with or without illumination resulted in a distinct increase in the levels of the pro-apoptotic proteins p53 and Bax respectively, while the expression of the pro-survival Bcl-2 decreased (Fig. 9).

Compared to SWNT-PVPk30, cells treated with SWNT-PEI under light illumination significantly decreased Bcl-2 levels and were accompanied by the up regulation of Bax and p53. Since cell survival in the early phase of apoptosis depends mostly on the balance between the pro- and anti-apoptotic proteins of the Bcl-2 family, the ratio of Bax/Bcl-2 acts as an important determinant of cell fate. Bax/Bcl-2 ratio increased significantly when cells treated with SWNT-PEI and SWNT-PVPk30 under illumination. These results clearly indicate that SWNT-PEI with illumination treatment increased the apoptosis signals in B16-F10 cells.

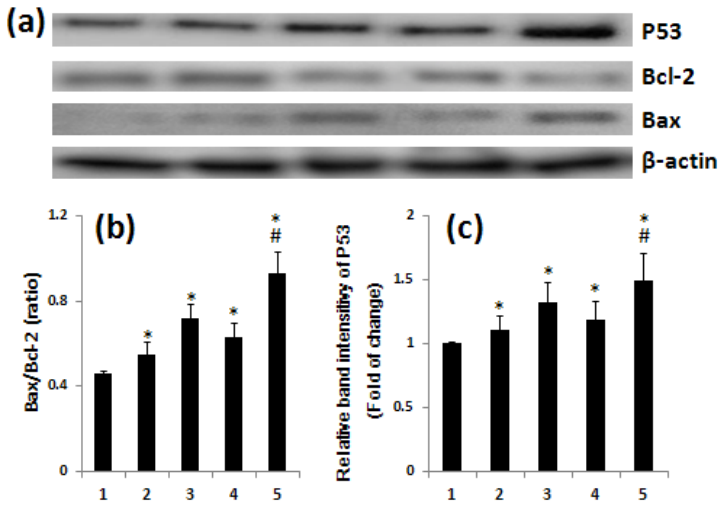

Fig. 9 Modulation of pro-and anti-apoptotic proteins by the SWNT-PEI and SWNT-PVPk30-treated cells. **(a)** Expression levels of p53, Bax and Bcl-2 in B16-F10 treated with SWNT-PEI or SWNT-PVPk30 were monitored by Western blotting. **(b)** and **(c)** Densitometric analysis of the expressions of p53 and Bax/Bcl-2 ratio. (Mean ± SD, n = 3, $p < 0.05$). (*) indicates statistically significant from control; ($^{\#}$) indicates statistically significant between SWNT-PEI and SWNT-PVPk30 groups.

3.7 Enhanced apoptosis of B16-F10 cells by SWNT-PEI with illumination

The intrinsic mitochondria pathway of apoptosis can be triggered by many

stimuli including ROS. Mitochondria is the major site of ROS production, and accumulation of ROS may lead to the initiation of apoptosis [36]. The toxicity of SWNTs has been extensively studied, however, studies on functionalized SWNTs with external stimuli leading to apoptosis are limited. In this study, we found that SWNT-PEI and SWNT-PVPk30 (SWNTs ≈ 50 μg/ml) with illumination treatment groups showed a time response of apoptosis to B16-F10 cells.

As shown in Fig. 10a, both SWNT-PEI and SWNT-PVPk30 caused a small amount of apoptosis without illumination, demonstrating that the illumination has no effect on apoptosis of B16-F10 cells. No significant difference was found between SWNT-PVPk30 with illumination group and SWNT-PEI with illumination group ($P > 0.05$) at 0.5 h. However, after 1 or 2 h illumination, SWNT-PEI resulted in a significant increase in apoptosis compared with SWNT-PVPk30 ($P < 0.05$) or control ($P < 0.05$). It is demonstrated that SWNT-PEI with illumination enhanced apoptosis of B16-F10 cells due to the stronger ROS-induced apoptosis by SWNT-PEI. With the duration of environmental stress, ROS levels can be increased dramatically as shown above. ROS may inflict damage to various cellular components, including DNA, protein and lipid members, which trigger apoptosis in cancer cells.

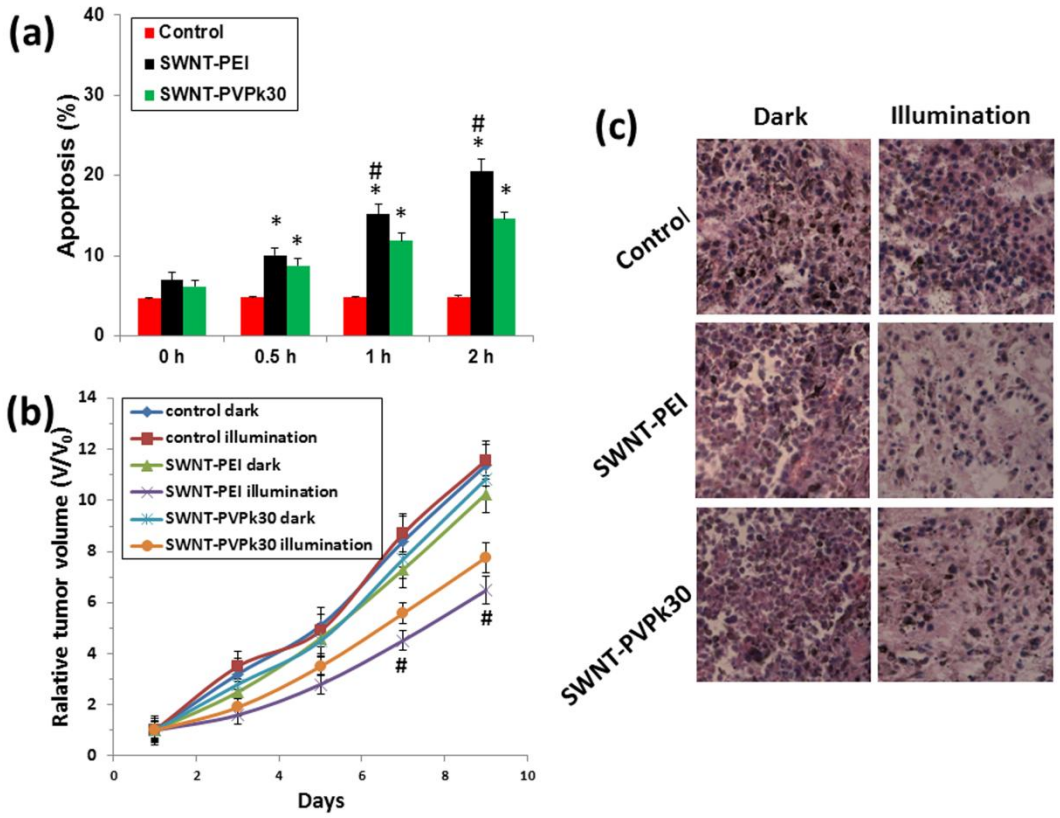

Fig. 10 **(a)** Apoptosis rate of B16-F10 cells with or without illumination. (Mean ± SD, n = 3, $p < 0.05$). (*) indicates statistically significant from control; ($^{\#}$) indicates statistically significant between SWNT-PEI and SWNT-PVPk30 groups. **(b)** Tumor growth of mice in different treatment groups within 10 days. (Mean ± SD, n = 5, $p < 0.05$). ($^{\#}$) indicates statistically significant between SWNT-PEI illumination and SWNT-PVPk30 illumination groups.. **(c)** H&E stained tumor tissues harvested from the mice with different treatments.

3.8 In vivo antitumor effect

To investigate in vivo PDT efficacy of SWNT-PEI and SWNT-PVPk30, comparative efficacy studies were conducted. The B16-F10 tumor-bearing mice were divided into 6 groups and were treated

The changes of relative tumor volume as a function of time were plotted in Fig. 10b. After 5 times treatment, control group with illumination showed a relative tumor

volume (V/V_0) of 11.57 ± 0.75. Control group, SWNT-PEI group and SWNT-PVPk30 group in dark showed a relative tumor volume (V/V_0) of 11.38 ± 0.83, 10.26 ± 0.84, 10.84 ± 0.72, respectively, suggesting that illumination alone and SWNT-PEI (or SWNT-PVPk30) without illumination would not affect the tumor growth. SWNT-PEI group and SWNT-PVPk30 group with illumination resulted in V/V_0 of 6.48 ± 0.55 and 7.77 ± 0.58

SWNT-PEI with illumination treatment group had tumor growth inhibition (TGI) of ~ 45%, it is significantly more effective than the other groups ($p < 0.05$). The results suggested that SWNT-PEI was used as a photosensitizer in PDT to achieve in vivo tumor treatment efficacy.

Histological analysis of tumor tissue in different treatment groups at day 10 post-treatment (Fig. 10c) reveals that no damage was found in tumors of control, SWNT-PEI and SWNT-PVPk30 group in dark, and control group with illumination. However, markedly increased apoptotic and necrotic tumor cells were observed in SWNT-PEI with illumination treatment groups, and furthermore a amount of cell death in tumor tissue was observed in the mice.

Recently, a number of groups have used C60 as a photodynamic therapy agent [37, 38], and some groups believed that C60 has the intrinsic singlet oxygen generation ability. However, our group found that SWNTs with suitable modification also could be used as a potential sensitizer for photodynamic therapy in vitro and in vivo.

4 Conclusions

To conclude, two types of functionalized SWNTs (SWNT-PEI and

SWNT-PVPk30) were successfully developed, which showed the characteristics of photodynamic effect under visible light illumination. SWNT-PEI has stronger photodynamic effect compared to SWNT-PVPk30 in vitro and in vivo, indicating that SWNT-PEI may be a potential sensitizer for PDT on cancers.

Acknowledgements

This work was supported by the National Natural Science Foundation of China under grant NO. 81302717, 81273451 and 81272527.

References

1. S. Akhter, I. Ahmad, M. Z. Ahmad, F. Ramazani, A. Singh, Z. Rahman, F. J. Ahmad, G. Storm and R. J. Kok, *Current cancer drug targets*, 2013, **13**, 362-378.
2. J. Guo, L. Bourre, D. M. Soden, G. C. O'Sullivan and C. O'Driscoll, *Biotechnol Adv*, 2011, **29**, 402-417.
3. D. Bartusik, D. Aebisher, A. Ghogare, G. Ghosh, I. Abramova, T. Hasan and A. Greer, *Photochem Photobiol*, 2013, **89**, 936-941.
4. J. Lin, S. Wang, P. Huang, Z. Wang, S. Chen, G. Niu, W. Li, J. He, D. Cui, G. Lu, X. Chen and Z. Nie, *ACS Nano*, 2013, **7**, 5320-5329.
5. G. Tian, W. Ren, L. Yan, S. Jian, Z. Gu, L. Zhou, S. Jin, W. Yin, S. Li and Y. Zhao, *Small*, 2013, **9**, 1929-1938, 1928.
6. A. L. Akopov, A. A. Rusanov, V. P. Molodtsova, I. V. Chistiakov, N. V. Kazakov, M. A. Urtenova, M. Rait and G. V. Papaian, *Khirurgiia (Mosk)*, 2013, 17-20.
7. S. L. Manoto, N. N. Houreld and H. Abrahamse, *Lasers Surg Med*, 2013, **45**, 186-194.
8. L. Milla Sanabria, M. E. Rodriguez, I. S. Cogno, N. B. Rumie Vittar, M. F. Pansa, M. J. Lamberti and V. A. Rivarola, *Biochim Biophys Acta*, 2013, **1835**, 36-45.
9. J. Kim, H. Jung, W. Lim, S. Kim, Y. Ko, S. Karna, O. Kim, Y. Choi and H. Choi, *J Oral Pathol Med*, 2013, **42**, 9-16.
10. L. Raj, T. Ide, A. U. Gurkar, M. Foley, M. Schenone, X. Li, N. J. Tolliday, T. R. Golub, S. A. Carr, A. F. Shamji, A. M. Stern, A. Mandinova, S. L. Schreiber and S. W. Lee, *Nature*, 2011, **475**, 231-234.
11. J. C. Ahn and P. S. Chung, *Gen Physiol Biophys*, 2012, **31**, 343-350.
12. D. M. Webster, P. Sundaram and M. E. Byrne, *European journal of pharmaceutics and biopharmaceutics : official journal of Arbeitsgemeinschaft fur Pharmazeutische Verfahrenstechnik e.V*, 2013, **84**, 1-20.
13. G. J. Bodwell, *Nat Nanotechnol*, 2010, **5**, 103-104.
14. C. Bi, M. Zhu, Q. Zhang, Y. Li and H. Wang, *J Nanosci Nanotechnol*, 2011, **11**, 1030-1036.

15. X. Zhang, M. Hu and D. Poulikakos, *Nano Lett*, 2012, **12**, 3410-3416.
16. J. Qiao, T. Hong, H. Guo, Y. Q. Xu and D. H. Chung, *Methods Mol Biol*, 2013, **1026**, 137-147.
17. D. Roxbury, A. Jagota and J. Mittal, *J Phys Chem B*, 2013, **117**, 132-140.
18. Z. Liu, F. Galli, W. J. Waterreus, E. Meulenbroek, R. I. Koning, G. E. Lamers, R. C. Olsthoorn, N. Pannu, T. H. Oosterkamp, A. J. Koster, R. T. Dame and J. P. Abrahams, *Chemphyschem*, 2012, **13**, 1569-1575.
19. L. Wang, J. Shi, H. Zhang, H. Li, Y. Gao, Z. Wang, H. Wang, L. Li, C. Zhang, C. Chen, Z. Zhang and Y. Zhang, *Biomaterials*, 2013, **34**, 262-274.
20. D. Crouzier, S. Follot, E. Gentilhomme, E. Flahaut, R. Arnaud, V. Dabouis, C. Castellarin and J. C. Debouzy, *Toxicology*, 2010, **272**, 39-45.
21. M. Pacurari, Y. Qian, W. Fu, D. Schwegler-Berry, M. Ding, V. Castranova and N. L. Guo, *J Toxicol Environ Health A*, 2012, **75**, 112-128.
22. L. Wang, M. Zhang, N. Zhang, J. Shi, H. Zhang, M. Li, C. Lu and Z. Zhang, *Int J Nanomedicine*, 2011, **6**, 2641-2652.
23. H. Asanuma, P. Subedi, J. Hartmann, Y. Shen, H. Mohwald, T. Nakanishi and A. Skirtach, *Langmuir*, 2013, **29**, 7464-7471.
24. F. Zhou, S. Wu, S. Song, W. R. Chen, D. E. Resasco and D. Xing, *Biomaterials*, 2012, **33**, 3235-3242.
25. A. L. Antaris, J. T. Robinson, O. K. Yaghi, G. Hong, S. Diao, R. Luong and H. Dai, *ACS Nano*, 2013, **7**, 3644-3652.
26. J. B. Miller, *J Chem Educ*, 1999, **76**, 592.
27. N. W. Kam, M. O'Connell, J. A. Wisdom and H. Dai, *Proc Natl Acad Sci U S A*, 2005, **102**, 11600-11605.
28. R. Dvash, A. Khatchatouriants, L. J. Solmesky, P. P. Wibroe, M. Weil, S. M. Moghimi and D. Peer, *J Control Release*, 2013, **170**, 295-305.
29. R. Singh, N. K. Mehra, V. Jain and N. K. Jain, *J Drug Target*, 2013, **21**, 581-592.
30. E. Heister, C. Lamprecht, V. Neves, C. Tilmaciu, L. Datas, E. Flahaut, B. Soula, P. Hinterdorfer, H. M. Coley, S. R. Silva and J. McFadden, *ACS Nano*, 2010, **4**, 2615-2626.
31. A. Beyerle, A. S. Long, P. A. White, T. Kissel and T. Stoeger, *Mol Pharm*, 2011, **8**, 976-981.
32. S. Gao, T. F. Chen, M. Y. Choi, Y. W. Liang, J. Y. Xue and Y. S. Wong, *Cancer Lett.*, 2013, **333**, 36-46.
33. H. M. Luo, A. M. Yang, B. A. Schulte, M. J. Wargovich and G. Y. Wang, *PLoS One*, 2013, **8**.
34. M. Dewaele, H. Maes and P. Agostinis, *Autophagy*, 2010, **6**, 838-854.
35. T. Murakami, H. Nakatsuji, M. Inada, Y. Matoba, T. Umeyama, M. Tsujimoto, S. Isoda, M. Hashida and H. Imahori, *J Am Chem Soc*, 2012, **134**, 17862-17865.
36. Y. H. Hsin, C. F. Chen, S. Huang, T. S. Shih, P. S. Lai and P. J. Chueh, *Toxicol Lett*, 2008, **179**, 130-139.
37. J. Shi, X. Yu, L. Wang, Y. Liu, J. Gao, J. Zhang, R. Ma, R. Liu and Z. Zhang, *Biomaterials*, 2013, **34**, 9666-9677.
38. K. O. Palyvoda, Grynyuk, II, S. V. Prylutska, A. A. Samoylenko, L. B. Drobot and O. P. Matyshevska, *Ukr Biokhim Zh*, 2010, **82**, 121-127.